Research Article | Vol. 33, No. 16 / 11 Aug 2025 / Optics Express 33342
Optics EXPRESS

Enhanced feedback sensitivity suppression in phase-detuned tunable lasers with high-Q Vernier-effect based ring resonators

YU XUE,* BIWEI PAN, YANG LIU, EMADREZA SOLTANIAN, JING ZHANG, GEERT MORTHIER, AND GUNTHER ROELKENS

Photonics Research Group, Department of Information Technology (INTEC), Ghent University - IMEC, Ghent 9052, Belgium
Yuyuxue.Xue@UGent.be

Abstract: The feedback sensitivity of a tunable laser with a highly wavelength-selective reflector using a high-Q Vernier-effect based ring resonator structure is examined through both experimental and simulation work. The study demonstrates that by properly tuning the amplitude and phase of the reflector, the laser exhibits reduced feedback sensitivity, leading to improved laser performance under external optical feedback. The onset of deterioration in the quantum-well-based laser due to optical feedback, characterized by excess relative intensity noise (RIN), is suppressed through red detuning to a feedback level above -13 dB, over 5 dB higher than for the non-detuned laser state. The study further characterizes the high-speed data transmission performance of the laser, showing that the red-detuned ring resonator based tunable laser offers enhanced stability against feedback. Simulation results confirm that the phase-detuned tunable laser, with its lower feedback coefficient, outperforms traditional distributed Bragg reflector (DBR) lasers, particularly under detuning conditions.

1. Introduction

The integration level of photonic integration circuits (PICs) is growing rapidly to match the increasing demand of data transmission networks. However, the presence of numerous optical components within a PIC introduces significant challenges, particularly due to reflections at the interfaces between these components, which can severely impact the performance of integrated semiconductor lasers. For intensity modulated laser diodes, the occurrence of coherence collapse is most detrimental as it leads to a severe increase in intensity noise. For many laser diodes (DFB and FP laser diodes in particular), this coherence collapse occurs when the feedback level increases to about -40 dB or -30 dB, depending on the laser diode length [1,2]. Consequently, the development of feedback-tolerant lasers and the mitigation of their coherence collapse has become the focus of recent research.

Various methods have been proposed to solve this problem, including the use of distributed Bragg reflector (DBR) lasers with long reflectors [3–6], of an on-chip isolator based on magneto-optic effects [7] or electro-optic modulation [8], and of self-injection locked lasers [9]. Among these approaches, detuned DBR lasers achieve feedback tolerance by shifting the lasing wavelength away from the Bragg wavelength to modify the effective linewidth enhancement factor, which is referred to as a phase-detuned laser in this paper. Moreover, long reflectors lead to large roundtrip times in the laser cavity, which reduce the feedback sensitivity even more [4]. This method offers an advantage by avoiding the need for additional structures beyond the laser cavity. Furthermore, for large-scale integrated circuits incorporating laser arrays, phase-detuned lasers are particularly promising due to their cost-effectiveness and ease of fabrication.

Several studies have analyzed the effects of phase detuning in DBR lasers [10,11]. Theoretical predictions indicate that the feedback coefficient is modified by a reduction factor, which depends

#561509 https://doi.org/10.1364/OE.561509
Journal © 2025 Received 5 Mar 2025; accepted 18 Jul 2025; published 30 Jul 2025

Optics EXPRESS

on the slope of both the amplitude and phase of the facet reflectivity as a function of wavelength [4,12]. DBR lasers with long Bragg sections and moderate κL value have a weak feedback sensitivity. However, it is very challenging to fabricate these long Bragg sections with uniform grating, while tuning of long Bragg sections also requires a lot of heating power. To overcome these issues, a phase-detuned laser with micro-ring resonators (MRRs) cavity is proposed. Due to its compact size and sharp falling edges in the reflectivity spectrum, the MRR has a strong potential to replace long Bragg reflectors.

To evaluate the performance of this type of laser, our research group has demonstrated tunable lasers based on MRRs by micro-transfer printing, a technology available under license from X-Celeprint Ltd., the III-V gain section [13,14]. In this paper, we investigate the static response and high-speed transmission characteristics of a tunable laser with a Vernier ring cavity under optical feedback. The laser is fabricated on a silicon nitride (SiN) platform, which supports high-Q-factor ring resonators. Our findings indicate that the laser exhibits strong feedback suppression under -13 dB optical feedback, demonstrating its potential for high-speed data transmission applications.

2. Principle of feedback sensitivity

The laser configuration considered in this section is schematically shown in Fig. 1. The laser consists of four main components: the high-reflection-coated (HR-coated) facet, with wavelength selective reflectivity, the gain and phase section, and the broadband low-reflectivity (AR-coated) facet. The phase section allows detuning the laser wavelength by heating the waveguide.

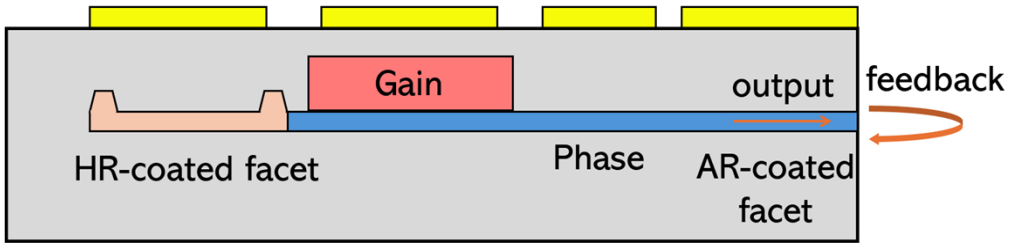

Fig. 1. Schematic of a detuned laser under external feedback.

To analyze the noise induced by the feedback light, we introduce the feedback coefficient C, derived by incorporating Langevin functions into the rate equations [4]:

$$C = \frac{\frac{1-R_1}{\sqrt{R_1}}\sqrt{R_e}\sqrt{1+\alpha^2}\tau_{ext}}{\tau_a - \frac{\lambda^2\partial\phi_2(\lambda)}{2\pi c\partial\lambda} - \frac{\alpha}{2}\frac{\lambda^2\partial\ln(R_2(\lambda))}{2\pi c\partial\lambda}} \tag{1}$$

where R_1, R_2, R_e represent the reflectivity of the AR-coated facet, the HR-coated facet, and the external feedback structure, respectively. α is the linewidth enhancement factor, which is determined by the active layer material. c is the velocity of light. τ_{ext} and τ_a are the roundtrip time of the external feedback and gain section respectively, and depend on the length of their cavities. $\phi_2(\lambda)$ denotes the frequency dependent phase of the HR-coated facet.

The feedback coefficient is a key parameter for evaluating a laser's tolerance to feedback. A lower feedback coefficient C indicates improved laser performance under external feedback. The numerator of Eq. (1) remains constant if the AR-coated facet maintains a stable reflectivity, as the linewidth enhancement factor and external feedback structure are independent of the laser. In the denominator, τ_a is constrained by the length of the gain section, which has an impact on the power consumption of the laser. The parameters $\phi_2(\lambda)$ and $R_2(\lambda)$ associated with the HR-coated facet, are among the most significant and adjustable factors in the laser design.

Optics EXPRESS

We compare two typical types of phase-detuned laser, where the HR-coated facet is composed of a Vernier MRR and a DBR, respectively, while maintaining the same gain section, AR-coated facet and external feedback structure to compare their feedback tolerance. Standard parameters used in the modelling of these lasers are shown in Table 1, assuming the passive waveguide is implemented in a low-loss SiN technology.

Table 1. Parameters of the standard configuration

Symbol	Description	MRR	DBR
R_1	reflectivity of AR-coated facet	30%	30%
R_e	reflectivity of external structure	0.1%	0.1%
a	linewidth enhancement factor	3	3
τ_{ext}	roundtrip time of the external feedback	10 ns	10 ns
τ_a	roundtrip time of the gain section	200 ps	200 ps
α_{wg}	loss of the passive waveguide	1.15 m^{-1}	1.15 m^{-1}
r	radius of the MRR	50 μm	\
l	length of the DBR	\	5 mm
κ_{MMR}	coupling coefficient of the MRR	0.02	\
κ_{DFB}	coupling coefficient of the DBR	\	400 m^{-1}
n_{eff}	effective index of the waveguide	1.81	1.81

The $R_2(\lambda)$ and $\phi_2(\lambda)$ of the MRR and DBR can be calculated using the parameters provided in Table 1. The reflectivity and phase of a Vernier MRR structure are obtained from the transmission T_{MMR} and the effective phase shift φ_{MMR} at the drop port of a single ring [15]:

$$R_2(\lambda) = T_{MRR}^4 = \left| \frac{\kappa_{MRR} exp\left(-\frac{1}{4}\alpha_{wg}L - i\frac{1}{2}\phi\right)}{1-(1-\kappa_{MRR})\exp\left(-\frac{1}{2}\alpha_{wg}L - i\phi\right)} \right|^8 \tag{2}$$

$$\phi_2(\lambda) = 4\varphi_{MRR} = -4\arctan\frac{Im\left(\sqrt{T_{MRR}}\right)}{Re\left(\sqrt{T_{MRR}}\right)} \tag{3}$$

where $\phi = \frac{2\pi}{\lambda} n_{eff} L$ is the single pass phase shift, and $L = 2\pi r$ is the round-trip length. $Im(T_{MRR})$ and $Re(T_{MRR})$ are the imaginary and real part of the transmission respectively.

For the DBR laser, the reflectivity and phase are given by [16]:

$$R_2(\lambda) = \frac{{\kappa_{DFB}}^2 sinh^2(\varepsilon l)}{\xi^2 sinh^2(\varepsilon l) + \varepsilon^2 cosh^2(\varepsilon l)} \tag{4}$$

$$\phi_2(\lambda) = -\arctan\left[\frac{\varepsilon}{\xi} cotanh(\varepsilon L)\right] \tag{5}$$

where $\varepsilon = \sqrt{{\kappa_{DFB}}^2 - \xi^2}$ and $\xi = 2\pi n_{eff}\left(\frac{1}{\lambda} - \frac{1}{\lambda_0}\right)$. λ_0 is the center wavelength of the Bragg grating.

Applying the parameters listed in Table 1 to Eq. (2) to (5), the reflectivity R_2 and phase ϕ_2 can be computed, as illustrated in Fig. 2(a) and Fig. 2(b), respectively. The reflectivity profile in Fig. 2(a) shows that the full width at half maximum of the MRR is significantly narrower than that of the DBR, indicating that the MRR contributes more to $\frac{\partial \ln(R_2(\lambda))}{\partial \lambda}$. In Fig. 2(b), the phase variation $\frac{\partial \phi_2(\lambda)}{\partial \lambda}$ for the MRR is most pronounced near the peak wavelength, whereas the DBR exhibits a broader phase variation. Due to its longer cavity length, the DBR provides consistent

Optics EXPRESS

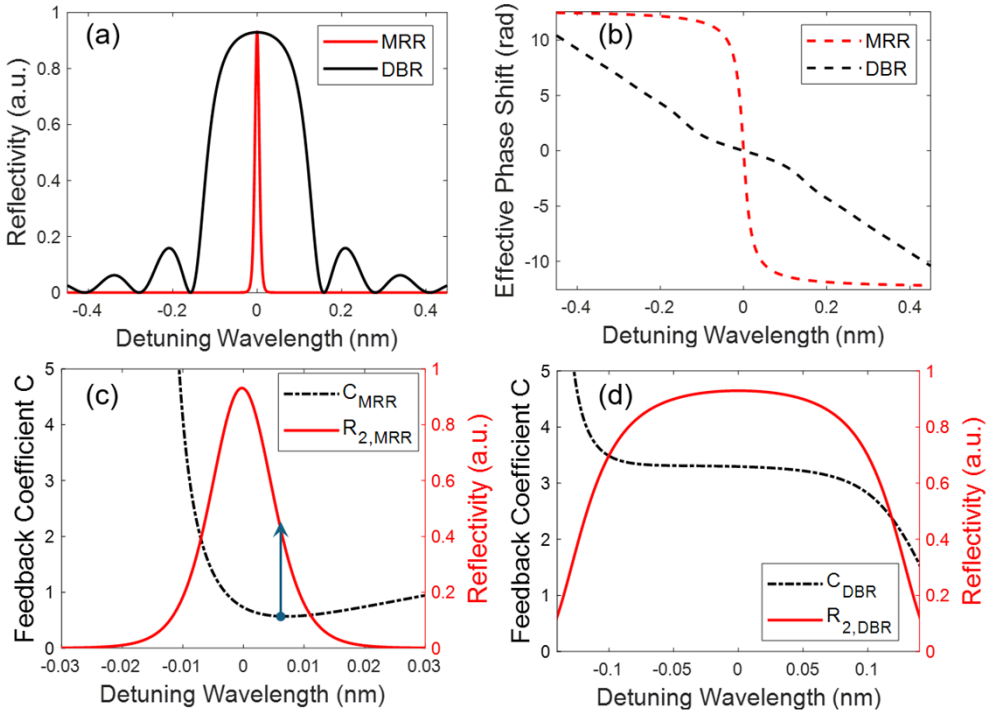

Fig. 2. Numerical simulation result of (a) the reflectivity R_2 of MRR and DBR, (b) the phase shift ϕ_2 of MRR and DBR, (c) the feedback coefficient of MRR with its reflectivity (the blue dot is located at the wavelength of minimized feedback coefficient on the solid-dot line) and (d) the feedback coefficient of the DBR with its reflectivity

feedback suppression by its phase variation. However, this increased length also leads to a larger laser footprint, which can be a limitation for large-scale integration.

Comparing the feedback coefficient C between MRR and DBR, as shown in Fig. 2(c) and Fig. 2(d), simulations reveal that the MRR has a lower baseline feedback coefficient near the center wavelength. When red-detuning is applied, the MRR achieves optimal performance around half of its peak reflectivity, highlighted by the blue dot and arrow in the figure. In contrast, the DBR does not attain similarly low feedback coefficient C within the stopband, constraining its detuning performance.

The simulation implies that a laser with a Vernier MRR under wavelength detuning achieves greater feedback suppression compared to a DBR laser.

3. Fabricated devices

Figure 3 illustrates the schematic diagram of the tunable laser with a Vernier ring mirror. The tunable laser consists of an 840-μm-long gain section, a phase section, and an HR(high-reflection) mirror section, which integrates two MRRs and a Sagnac loop reflector. Additionally, it includes a tunable-reflection mirror section featuring a Mach-Zehnder interferometer (MZI) with another Sagnac loop reflector, as the outcoupling mirror. To provide gain in the laser cavity, an InP coupon with a multi-quantum well (MQW) active layer is micro-transfer printed onto the top of a hydrogenated amorphous silicon (a-Si:H) waveguide that couples the mode to the SiN waveguide layer below. The passive optical components of the laser cavity are fabricated using low-loss SiN waveguides, supporting high-Q-factor MRRs (loaded Q-factor of 47,300 in the

Optics EXPRESS

experiment). Ti/Au layers are deposited on top of the two MRRs and waveguides to function as heaters, enabling phase tuning. The phase section, situated between the gain section and the HR mirror section, consists of a straight waveguide covered with a heater, which allows for wavelength tuning of the laser.

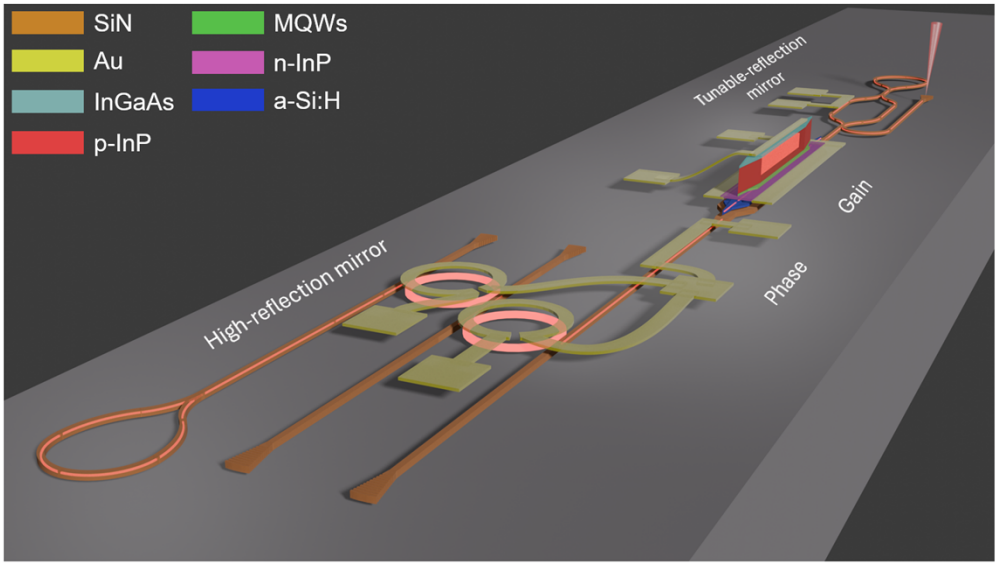

Fig. 3. Schematic diagram of the tunable laser.

When current is applied to the electrodes of the gain section, the laser coupon initiates spontaneous emission. This emission is spectrally filtered by the Vernier ring, and optical feedback between the two cavity mirrors establishes resonance. The lasing wavelength is determined by the effective cavity length and the transmission response of the Vernier ring, both of which can be tuned via integrated heaters on the phase section and the MRRs. The Vernier ring comprises two rings with slightly different radii, enabling a broader wavelength tuning range through the Vernier effect. Once the resonance condition stabilizes, the output port provides single-mode emission with a fixed wavelength and stable output power.

The wavelength detuning is achieved by varying the power applied to the heater on the phase section, as shown in Fig. 4. A temperature controller with a water-cooling system is employed beneath the chip to minimize environmental disturbances and ensure thermal stability in other regions of the device during tuning. The efficiency of the detuning process is constrained by the low thermo-optic coefficient and the length of the SiN waveguide in this device. The decrease in output power reflects the increased mirror loss of the laser as the lasing wavelength is detuned from the transmission peak of the MRRs, which can also induce mode instability and elevate the lasing threshold with further detuning.

4. Experimental results of feedback suppression

The optical feedback sensitivity of the device is examined by measuring its RIN, linewidth, and high-speed data transmission performance under varying feedback levels. Figure 5 presents the experimental setup used to characterize the laser's performance under external feedback. Six probes are connected to the pads on the device under test (DUT) to control the wavelength detuning, the phase of the MRRs, and to supply current to the gain section. The optical feedback in the measurement is introduced by placing a circulator at the output port, which redirects a

Optics EXPRESS

portion of the light back to the DUT. Erbium-doped fiber amplifiers (EDFAs) in the feedback path are used to compensate for losses caused by the grating coupler and splitter. The optical signal is routed through a polarization controller (PC) to optimize the polarization state for coupling back into the chip. The RIN of the laser is measured using an electrical signal analyzer (ESA, Rohde & Schwarz FSP).To characterize the linewidth, a laser linewidth analyzer (OEwaves OE4000) is employed.

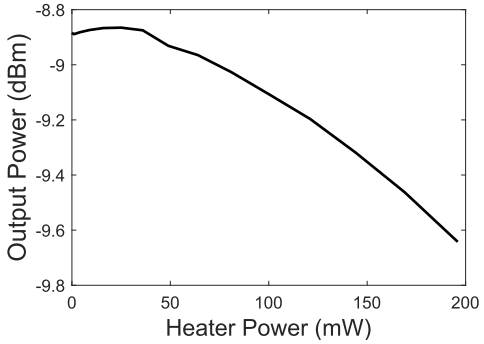

Fig. 4. Output power of the tunable laser vs. heating power applied to the phase section.

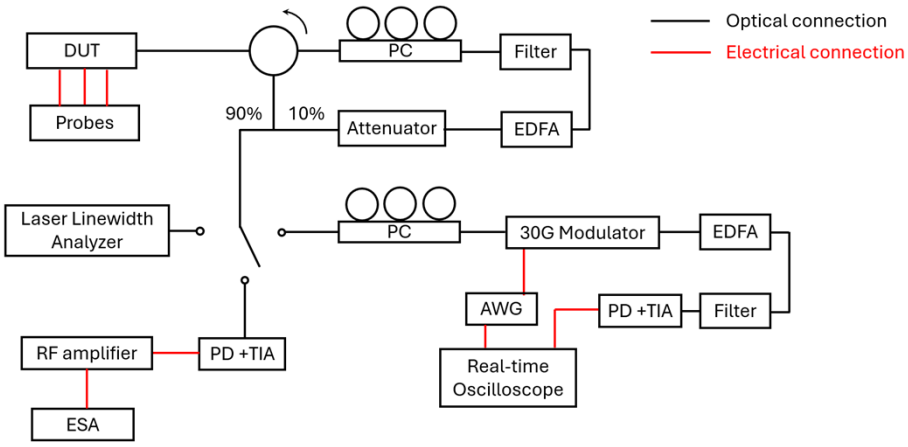

Fig. 5. Setup used for the measurements.

For high-speed modulation analysis, an arbitrary waveform generator (AWG, Keysight M9502A) drives a 30 GHz electro-optic modulator to modulate the laser output. The modulated signal is amplified with an EDFA and filtered to ensure sufficient power for the eye diagram measurement. A high-speed photodiode (PD) with a transimpedance amplifier (TIA) converts the optical signal into an electrical signal, which is then analyzed using a real-time oscilloscope (Agilent, DCA-X 86100D). The eye diagram is extracted to evaluate the laser's data transmission performance under feedback.

The RIN performance of the laser is initially characterized using the setup. The data obtained from the ESA is then substituted into the formula to calculate the RIN [17],

$$RIN = \frac{N_{on}(f) - N_{off}(f)}{GR_L I_R^2 \Delta f} \tag{6}$$

Optics EXPRESS

where $N_{on}(f)$ and $N_{off}(f)$ represent the noise power measured by the ESA and the noise power originating from the photodetector and amplifier, respectively; G is the gain of the amplifier; R_L and I_R denote the load resistance and the photocurrent of the photodetector; and Δf is the measurement bandwidth.

Figure 6(a) presents the RIN sweep results with feedback levels ranging from -80 dB to -13 dB and detuning power (heater power) ranging from 0 mW to 144 mW (estimated wavelength detuning from 0 pm to 5.9 pm). These results are derived by averaging the RIN measurements between 80 MHz and 2 GHz. Coherence collapse in the laser with zero detuning occurs when the feedback level increases to approximately -20 dB, which is an improvement compared to the DBR laser reported in previous studies [1]. This high feedback tolerance is attributed to the lower base feedback coefficient C, as evidenced by the comparison between the high-Q ring and DBR in Fig. 2. The detuning performance effectively suppresses the feedback further, even when the feedback reaches -13 dB. The frequency range from 80 MHz to 2 GHz encompasses the region where coherence collapse is visible in the spectrum, as illustrated in Fig. 6(b). The noise floor around -125 dB/Hz, shown in the figure, is limited by the instruments in the experimental setup. Figure 6(b) clearly indicates that the coherence collapse, with high RIN at frequencies below 2 GHz, has occurred at -13 dB feedback for 0 and 80 mW heating power (and hence little detuning), but that this deterioration induced by coherence collapse is suppressed for 144 mW heating power (and larger detuning) at the same feedback level.

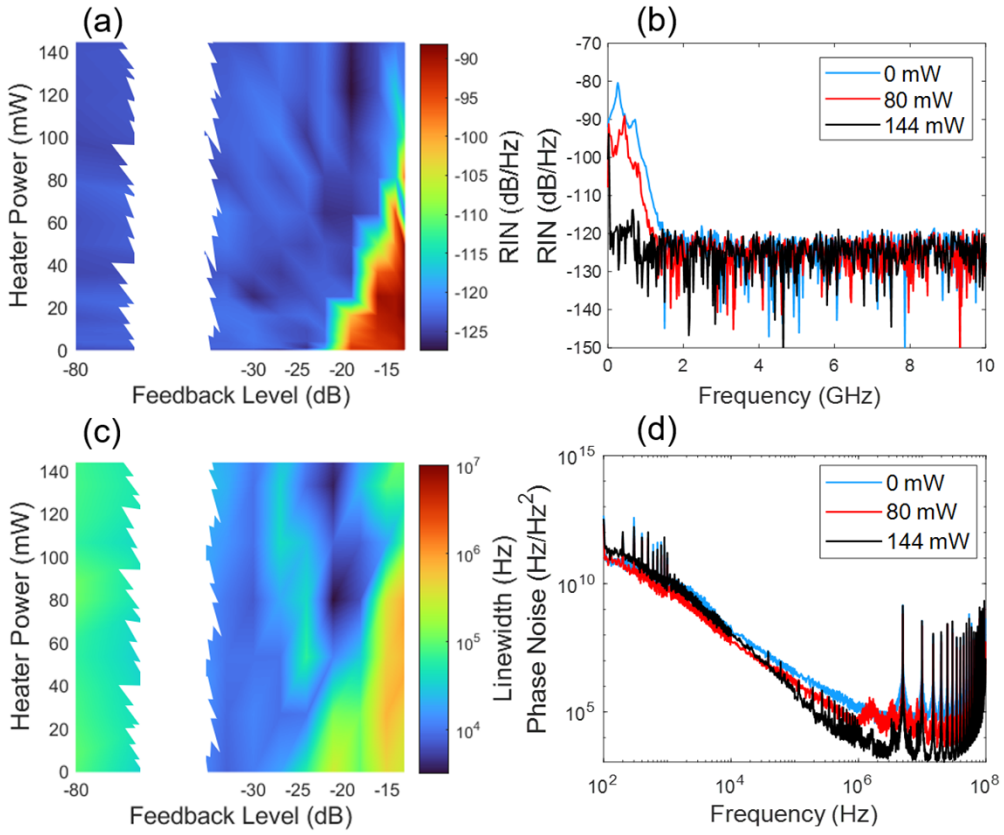

Fig. 6. 2-dimensional sweep diagram of (a) average RIN and (c) linewidth under different feedback level and detuning power, with (b) RIN response of the laser under -13 dB feedback with 0 mW, 80 mW, 144 mW detuning power and (d) frequency noise under-13 dB feedback with 0 mW, 80 mW, 144 mW detuning power.

Optics EXPRESS

The linewidth of the laser is further characterized in Fig. 6(c). The linewidth without feedback is approximately 100 kHz, while with appropriate feedback level and suitable detuning, the linewidth narrows to 3.5 kHz. The linewidth suffers equally from the onset of coherence collapse as the RIN, but with a different dependence on the detuning and heating power than the RIN.

The high-speed performance of the laser for varying detuning of the wavelengths and under -13 dB feedback is characterized by its eye diagram, as shown in Fig. 7. In the absence of detuning, coherence collapse leads to significant noise in the data transmission. However, when the power applied to the heater reaches 48 mW, the eye diagram improves, as the noise induced by the feedback is suppressed by the detuning of the Vernier ring. As the heater power increases, indicating red detuning of the wavelength, the quality of the eye diagram approaches that observed without feedback. These results demonstrate that detuning provides effective suppression of feedback in the laser.

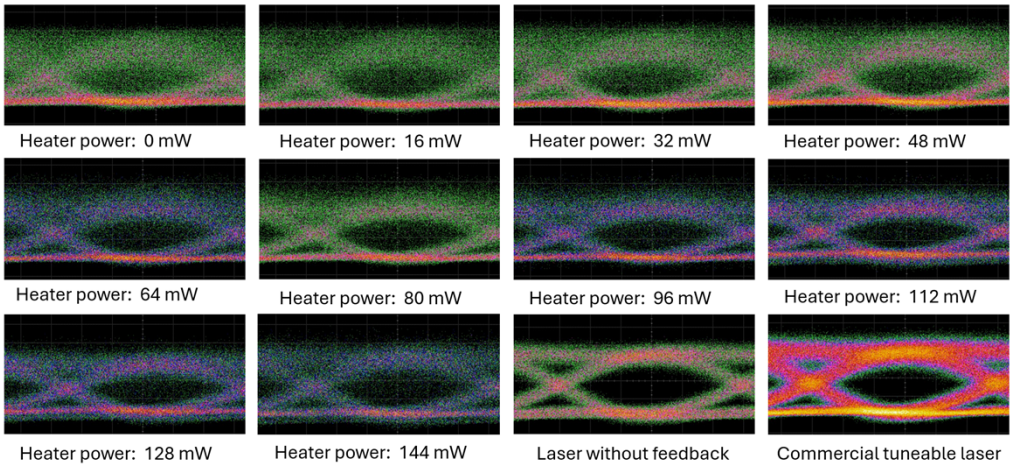

Fig. 7. Eye diagram of the laser with 30 Gb/s data transmission under different laser detuning and under -13 dB feedback. The last two figures show the eye diagram of the fabricated laser and of a commercial tunable laser (Santec TSL510) without feedback using the same setup.

5. Conclusion

In summary, we have investigated the feedback sensitivity of a tunable laser incorporating two high-Q MRRs in a reflector. The results demonstrate that this laser exhibits reduced feedback sensitivity when the laser is properly detuned. The excess RIN and deterioration induced by optical feedback were suppressed through red detuning at a feedback level of -13 dB, compared to the non-detuned operating state, where a feedback level of -20 dB caused coherence collapse, as also verified in a high-speed transmission experiment. This research highlights the potential of tunable lasers incorporating two or more MRRs in a reflector. By detuning the micro ring resonators via a microcontroller unit, a high feedback tolerance can be obtained, which could be taken advantage of in future large-scale photonic integrated systems-on-chip.

Funding. Interreg Vlaanderen-Nederland (LIGHTUP); Nationaal Groeifonds (PhotonDelta).

Disclosures. The authors declare no conflicts of interest.

Data Availability. Data underlying the results presented in this paper are not publicly available at this time but may be obtained from the authors upon reasonable request.

Optics EXPRESS

Reference

1. R. Tkach and A. Chraplyvy, "Regimes of feedback effects in 1.5-μm distributed feedback lasers," J. Lightwave Technol. **4**(11), 1655–1661 (1986).
2. K. Petermann, *Laser Diode Modulation and Noise* (Springer Dordrecht, 1988), Vol. 3.
3. V. Tronciu, N. Werner, H. Wenzel, *et al.*, "Feedback Sensitivity of Detuned DBR Semiconductor Lasers," IEEE J. Quantum Electron. **57**(5), 1–7 (2021).
4. G. Morthier, "Feedback Sensitivity of DBR-Type Laser Diodes," IEEE Photonics J **13**(4), 1–5 (2021).
5. Q. Yang, D. Lu, Y. He, *et al.*, "High Optical Feedback Tolerance of a Detuned DBR Laser for 10-Gbps Isolator-Free Operation," Photonics **10**(1), 38 (2023).
6. Y. Matsui, R. Schatz, D. Che, *et al.*, "Isolator-Free > 67-GHz Bandwidth DFB Plus R Laser with Suppressed Chirp," *Optical Fiber Communications Conference and Exposition* (OFC, 2020).
7. S. Liu, D. Minemura, and Y. Shoji, "Silicon-Based Integrated Polarization-Independent Magneto-Optical Isolator," Optica **10**(3), 373–378 (2023).
8. M. Yu, R. Cheng, C. Reimer, *et al.*, "Integrated Electro-Optic Isolator on Thin-Film Lithium Niobate," Nat. Photonics **17**(8), 666–671 (2023).
9. C. Xiang, W. Jin, O. Terra, *et al.*, "3D Integration Enables Ultralow-Noise Isolator-Free Lasers in Silicon Photonics," Nature **620**(7972), 78–85 (2023).
10. Y. Matsui, R. Schatz, D. Che, *et al.*, "Low-Chirp Isolator-Free 65-GHz-Bandwidth Directly Modulated Lasers," Nat. Photonics **15**(1), 59–63 (2021).
11. M. Happach, D. de Felipe, V. N. Friedhoff, *et al.*, "Effect of Optical Feedback on the Wavelength Tuning in DBR Lasers," J. Lightwave Technol. **38**(17), 4824–4833 (2020).
12. X. Pan, H. Olesen, and B. Tromborg, "A Theoretical Model of Multielectrode DBR Lasers," IEEE J. Quantum Electron. **24**(12), 2423–2432 (1988).
13. B. Pan, J. Bourderionnet, V. Billault, *et al.*, "III-V-on-Si_3N_4 Widely Tunable Narrow-Linewidth Laser Based on Micro-Transfer Printing," Phot. Res. **12**(11), 2508–2520 (2024).
14. E. Soltanian, G. Muliuk, S. Uvin, *et al.*, "Micro-Transfer-Printed Narrow-Linewidth III-V-on-Si Double Laser Structure with a Combined 110 nm Tuning Range," Opt. Express **30**(22), 39329–39339 (2022).
15. W. Bogaerts, P. De Heyn, T. Van, *et al.*, "Silicon Microring Resonators," Laser Photonics Rev. **6**(1), 47–73 (2012).
16. Y. O. Barmenkov, D. Zalvidea, S. Torres-Peiro, *et al.*, "Effective Length of Short Fabry-Perot Cavity Formed by Uniform Fiber Bragg Gratings," Opt. Express **14**(14), 6394–6399 (2006).
17. M. Fukuda and G. Mura, "Laser Diode Reliability," in *Advanced Laser Diode Reliability* (Elsevier, 2021), pp. 1–49.